

Evidence for double-electron excitations in the L_3 -edge x-ray absorption spectra of actinides

Christoph Hennig

Forschungszentrum Dresden-Rossendorf, Institute of Radiochemistry, D-01314 Dresden, Germany
(Received 26 July 2006; revised manuscript received 25 September 2006; published 17 January 2007)

A double-electron excitation in L_3 -edge x-ray absorption spectra of actinides has been observed for the first time. The investigation of this effect is presented. Actinide species in valence states IV and III were investigated by using experimental data of Th^{4+} , U^{4+} , Np^{4+} , Pu^{3+} , and Am^{3+} hydrates. The double-electron excitation was identified as a $L_3N_{6,7}$ shake-up effect. Energy positions of the double-electron features were found in good agreement with the $Z+1$ approximation. The LN resonance intensity corresponds with the resonance of the L edge. This has been observed by comparing the L_1 , L_2 , and L_3 XANES spectra of Th^{4+} , as well as the L_3 XANES spectra of Np in oxidation states IV, V, VI, and VII. Influences of the double-electron excitation on the EXAFS signal are discussed.

DOI: [10.1103/PhysRevB.75.035120](https://doi.org/10.1103/PhysRevB.75.035120)

PACS number(s): 78.70.Dm, 78.70.Ck, 61.10.Ht, 79.60.Bm

I. INTRODUCTION

The inner-shell photoexcitation of an electron is often accompanied by the excitation of secondary electrons with lower binding energies. These electrons can be excited into unoccupied states (shake up) or ejected into the continuum (shake off). Such processes are revealed as satellite lines in x-ray fluorescence and photoelectron spectra. X-ray absorption spectra yield directly the energy level of the multielectron excitations in noble gases whose atomic absorption is modulated by discrete resonances and slope modifications. Multielectron resonances have been observed above the K edge of Ne,¹ Xe,² Ar,³ and Kr (Ref. 4) but also above their L edges.⁵ In noble gases, the absorption signal is not affected by photoelectron backscattering effects from neighbored atoms that cause the extended x-ray absorption fine structure (EXAFS). To describe multielectron resonances created by excitation energies far from the transition onset, the sudden approximation is appropriate.⁶ This approximation regards the ionization process as rapid enough that the outer electrons remain passive and do not rearrange themselves in presence of an inner vacancy. If the excitation energy is close to the second electron energy, the excited atom undergoes an adiabatic relaxation. The primary photoelectron has in this situation only a low kinetic energy, it leaves the atom relative slowly and the cross section of the multielectron excitation is reduced. The x-ray absorption process can reach the adiabatic limit and shows therefore often only weak multielectron resonances. Nevertheless, although the single-electron EXAFS oscillation is able to cover double-electron excitations, they have been also revealed in the spectra of liquids and solids. As example, solid compounds of the third period show KL multielectron transitions, e.g., α -Si (Ref. 7) and salts of P, S, and Cl.⁸ Ca^{2+} hydrate, as example of the fourth period, shows KM_1 and $KM_{2,3}$ resonances.⁹ For fifth period, multielectron transitions has been observed at the KN_1 , $KM_{4,5}$, and $KM_{2,3}$ edges of gaseous Br_2 and HBr .¹⁰ In the sixth period, e.g., for the lanthanides, the resonances are associated with $LN_{4,5}$ edges.^{11,12}

Up to now it has not been investigated whether the actinides, as members of the seventh period, show also multielectron excitations. The low vapor pressure and radio pro-

tection aspects prevent investigations in the gas phase. In the last decade, several EXAFS data of actinides in aqueous solution have been published with the aim to reveal their near-order structure. A part of these spectra will be reinvestigated here with regard to multielectron features.

The paper is organized as follows. In Sec. II the experimental details are described. In Sec. III A the scattering effects from the neighbors are presented. In Sec. III B the evidence of the double-electron excitation is shown and their origin is discussed. Section III C describes the fine structure of the feature. Consequences for the EXAFS data analysis are discussed in Sec. III D.

II. EXPERIMENTAL DETAILS

The x-ray absorption data were collected on the Rossendorf Beamline¹³ at the ESRF, Grenoble. The monochromator is equipped with Si(111) double crystals. Higher harmonics were rejected by two Pt coated mirrors and a detuned second monochromator crystal. The spectra were collected in transmission mode using argon-filled ionization chambers. Across the absorption edge data points were taken in steps of 1.0 eV, and across the EXAFS region data points have equidistant k steps of 0.05 \AA^{-1} . For fine structure measurements across the double-electron feature, energy steps of 1.0 eV were applied. The monochromator energy scale was calibrated according to the K edge of a Y metal foil. As reference for the Y 1s ionization energy served the first inflection point of the absorption edge at 17 038.0 eV. The XAFS data were reduced as follows. First, a polynomial function, fitted to the preedge region, was subtracted from the entire data set. The atomic background above the absorption edge, $\mu_0(E)$, was approximated by a spline function. The fine structure, $\chi(E)$, was obtained from the raw data $\mu(E)$ by $\chi(E) = [\mu(E) - \mu_0(E)] / \mu_0(E)$, converted to $\chi(k)$ and weighted with k^3 . Data extraction and EXAFS fits were performed using WINXAS (Ref. 14) and EXAFSPAK (Ref. 15) software. The EXAFS data were fit using theoretical phase and amplitude functions calculated with the FEFF 8.2 code.¹⁶ The fine structure of the multielectron transition was separated from the signal by subtracting the data of EXAFS shell fit from the experimental data.

TABLE I. Sample overview.

Sample	Actinide	Solution
Np ⁴⁺	0.05 M Np(IV)	0.1 M HNO ₃
Np ⁵⁺	0.05 M Np(V)	0.1 M HNO ₃
Np ⁶⁺	0.05 M Np(VI)	0.1 M HNO ₃
Np ⁷⁺	0.015 M Np(VII)	2.5 M NaOH
Th ⁴⁺	0.05 M Th(IV)	0.5 M HClO ₄
U ⁴⁺	0.01 M U(IV)	0.1 M HClO ₄
Pu ³⁺	0.05 M Pu(III)	1.0 M HClO ₄
Am ³⁺	0.01 M Am(III)	1.0 M HClO ₄

An overview of the samples used in this study is given in Table I. The preparation conditions have been described previously.^{17–19} All solutions were filled in polyethylene cuvettes with an optical path length of 13 mm, and encapsulated in a second hot sealed polyethylene bag. The XAFS measurements were performed at 25 °C.

III. RESULTS AND DISCUSSION

A. EXAFS background signal

Double-electron excitations are usually associated with slope changes and anomalous structures in the atomic background of the x-ray absorption cross section. Noble gases and monoatomic metal vapor^{20,21} are appropriated to investigate these effects, whereas condensed systems suffer from the backscattering of the photoelectron wave by the coordinated neighbor atoms. This backscattering phenomenon, the x-ray absorption fine structure (EXAFS), is usually described in a one-electron spherical wave theory.²² The backscattering amplitude increases with the number of neighbors N_{ij} as well as with their atomic number Z . High N_{ij} and Z values, such as in metals, are related with large single-electron backscattering amplitudes. For several elements with higher Z number, where the low vapor pressure does not allow measurements in the gas phase, multielectron effects were revealed in ionic compounds or aqueous solutions.¹² Hydrates, who are the dominating species in aqueous solution at low pH values, are only associated with water molecules by electrostatic interactions. The thermal movement of the associated ligands results partly in destructive interference effects in the single-electron scattering amplitude. Such systems are well suited for the study of multielectron resonances.

The actinide elements show numerous oxidation states in particular for the elements Np to Pu, where they range from III to VII. The electronic structure involves besides $6d$ states partly filled $5f$ shells. The $5f$ states are less strictly located than the $4f$ states of the lanthanides, and can therefore participate in the chemical bond. This electronic configuration affects the physical and chemical properties and poses a large variation in the coordination geometry. In oxidation state V and VI, the actinides U, Np, Pu, and Am occur mainly as transdioxo cations, AnO_2^{n+} ($n=1$ and 2).²³ These transdioxo bonds are strongly covalent having the character of a triple bond.²⁴

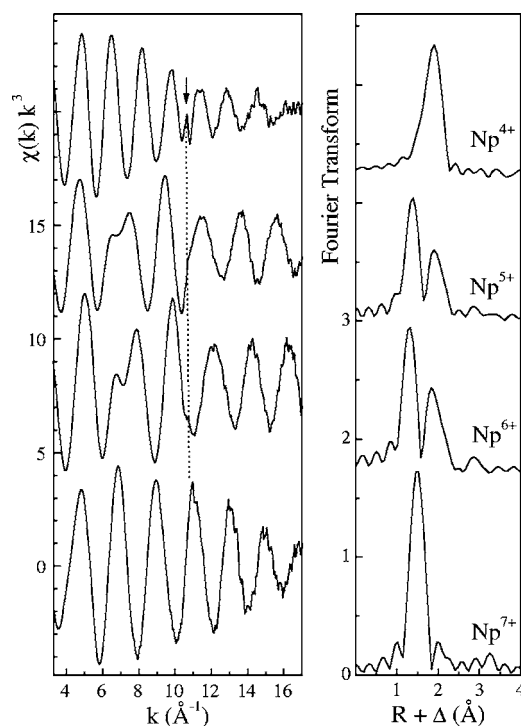


FIG. 1. Np L_3 -edge k^3 weighted EXAFS data (left) of Np⁴⁺, Np⁵⁺, Np⁶⁺, and Np⁷⁺ and their corresponding Fourier transforms (right). The FT is shown in the k range 3.3–13 \AA .

Although the species in aqueous solution are expected to be appropriate for investigating multielectron effects, a closer inspection revealed limitations in presence of actinyl ions. As an example, the k^3 weighted L_3 -edge EXAFS spectra of Np in different oxidation states are shown in Fig. 1 together with their corresponding Fourier transforms. The modulus of the Fourier transform represents the pseudoradial distribution of the next neighbor atoms. The Fourier transform is not corrected for the scattering phase shift, so that the peaks are shifted with respect to the true distance R . Table II summarizes the obtained coordination numbers and atomic distances in the first coordination shells. For actinide aquo ions in oxidation state III and IV, coordination numbers between 7 and 12 are observed.^{19,25–27} The Np⁴⁺ hydrate, present here, is coordinated by 9 water molecules with a Np–O distance of 2.406 \AA . Its single oxygen coordination shell is related with a sinusoidal oscillation in $\chi(k)$. A quantitative data analysis of Np⁵⁺ and Np⁶⁺ has been published by Reich *et al.*¹⁷ The coordination polyhedron of Np⁵⁺ and Np⁶⁺ shows two axial arranged transoxygen atoms (O_{ax}), completed by 4 and 5 equatorial oxygen atoms (O_{eq}), respectively. With increasing central atom charge, the bond lengths are shortened around 0.07 \AA . A beat node feature occurs in the $\chi(k)$ at $\sim 7 \text{\AA}^{-1}$ due to the superposition of axial and equatorial scattering contributions. Structural parameters of aqueous Np⁷⁺ hydroxid has been published by Bolvin *et al.*²⁸ It has been shown that the coordination polyhedron comprises four covalent oxygen atoms with a Np–O distance of 1.89 \AA . These actinyl oxygen atoms dominate the scattering signal. The coordination polyhedron of $NpO_4(OH)_2^{3-}$ comprises two OH^- ions with a Np–O distance of 2.32 \AA .

TABLE II. EXAFS structural parameters for Npⁿ⁺ species.

Sample	Shell	R [Å]	N_{ij}	σ^2 [10^{-2} Å ²]	Ref.
Np ⁴⁺	Np–O	2.406±0.002	8.9±0.2 ^a	0.68±0.02	This work
Np ⁵⁺	Np=O	1.822±0.003	1.9±0.2	0.23±0.03	17
	Np–O	2.488±0.009	3.6±0.6	0.6±0.1	
Np ⁶⁺	Np=O	1.754±0.003	2.0±0.1	0.15±0.03	17
	Np–O	2.414±0.006	4.6±0.6	0.56±0.09	
Np ⁷⁺	Np=O	1.89±0.04	3.6±0.3	0.20	28
	Np–OH	2.32±0.03	3.3±1.3	1.33	

^a $\sigma_0^2=0.9$, R —distance, N_{ij} —coordination number, σ^2 —Debye-Waller factor.

It is obvious, that the scattering amplitude at higher k range is much more pronounced in presence of actinyl oxygen atoms, than in their absence. The reason is, that the EXAFS amplitude, which is related to the next-neighbor distance with $1/R^2$, is stronger affected by the close located actinyl ions than by the water molecules. In each spectrum anomalous features are observed, indicated in Fig. 1 by an arrow and a dotted line. The most significant feature occurs for Np⁴⁺. Weak anomalous structures can be also indicated on the right side of the EXAFS oscillation for Np⁵⁺, on the left side for Np⁶⁺, and on top of the oscillation maximum for Np⁷⁺; but their appearance is less pronounced in relation to the anomalous feature visible in the spectrum of Np⁴⁺. Similar effects were observed also for other actinyl ions. Therefore, at least under the applied conditions, actinide species with strong covalent coordinated oxygen atoms are less appropriated for the study of multielectron effects than species with a one single hydrate coordination sphere. In order to investigate the nature of this anomalous feature only actinide ions in valence states III and IV were considered in this study.

B. Experimental evidence for double-electron excitation

The L_3 -edge k^3 EXAFS spectra of different actinide hydrates in aqueous solution ($An^{n+}=Th^{4+}, U^{4+}, Np^{4+}, Pu^{3+}$, and Am^{3+}) are reported in Fig. 2. The signal is formed by a single-frequency sinusoidal oscillation without beat nodes. A difference in the amplitude and frequency among the spectra of An^{4+} and An^{3+} is clearly visible. This is related with the differences in the An–O distances as described elsewhere.²⁹ In the k range 9.8–11.2 Å^{−1} small anomalous features appear superimposed to the main oscillations. These features are indicated individually by arrows. Their position appears shifted to higher k values with increasing atomic number Z . All features show a relative sharp maximum. Sharp, resonancelike absorption features appear only if the core electron excitation is accompanied by a shake up of the second electron to a bound state. In contrast, the cross section appears gradually increased with increasing photon energy, if both electrons are excited to the continuum.³⁰ Therefore, the sharp features in Fig. 2 are originated by a shake up process.

In order to assign the experimental features to a specific electron excitation channel, the difference between the energy of the anomalous maximum E_f and the energy of the

absorption edge threshold, E_0 , was estimated. The energy position of the anomalous maximum E_f is taken directly from the raw data, without fitting and subtracting the $\chi(E)$ background signal. Their energies are listed in Table III. The L_3 absorption edge energy, i.e., the ionization energy, is superimposed by transitions of the $2p_{3/2}$ core electron to unoccupied nd states and continuum ed states. Several procedures are in use to obtain experimental values for E_0 from the absorption spectrum: (i) The threshold region can be deconvoluted by an arctangent function describing the transition into the continuum, and at least one Lorentz function representing the transition into the nd states.^{12,31,32} This data treatment suffers from the strong correlation between the arctangent and the Lorentz function that needs to include

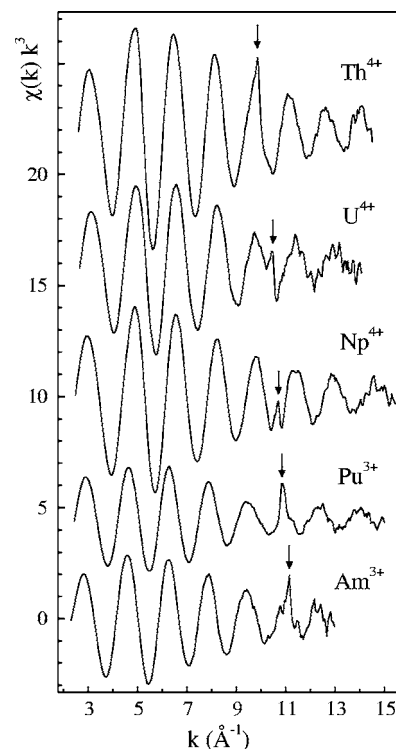


FIG. 2. Experimental k^3 weighted extended x-ray absorption fine structure at the L_3 edge of Th^{4+} , U^{4+} , Np^{4+} , Pu^{3+} , and Am^{3+} hydrate. Arrows indicate the maximum of the double-electron excitation. The energy values of these features are given as E_f in Table III.

TABLE III. Listing of the L_3 -edge energy E_{1st} , the difference between the white line energy and the L_3 -edge energy ΔE_{WL-1st} , and the energy of the anomalous feature, E_f . For comparison, the theoretical estimated value of the L_3 -edge energy to produce a single inner vacancy, L_3^{theo} , according Deslattes *et al.* (Ref. 42) is listed. All values are given in eV.

Z	An^{n+}	E_{1st}	ΔE_{WL-1st}	L_3^{theo}	E_f
90	Th ⁴⁺	16301.8	3.6	16310.3	16678.8
92	U ⁴⁺	17171.8	3.7	17174.4	17594.7
93	Np ⁴⁺	17613.6	3.9	17616.9	18061.2
94	Pu ³⁺	17057.9	4.2	18060.1	18518.6
95	Am ³⁺	18512.7	4.4	18514.4	18995.4

some arbitrary constraints. Neglecting such constraints, the position of the arctangent function can easily shift above the Lorentz maximum, which may not reflect the true edge position. (ii) An analysis of the EXAFS oscillations using phase functions from SCF codes allow to determine the origin of the wave vector k as ionization energy $E_{k=0}$.^{33,34} Especially for low k range, this procedure depends on the chosen potentials and can lead to energy differences >10 eV among different oxidation states. (iii) A common procedure is the use of the first maximum of the derivative of the raising edge, E_{1st} . The reproducibility of this procedure is in the range of 0.3 eV, but the value is expected to be up to ~ 2 eV too high in relation to the true edge energy. Because this systematic energy shift seems to be a tolerable deviation for the purpose of this study, the energy value of E_{1st} is used for E_0 . The estimated values of E_{1st} are given in Table III and the corresponding L_3 -edge XANES spectra are shown in Fig. 3.

The energy for the electron shell, which is related with the shake-up transition E_S , was estimated by the difference of the

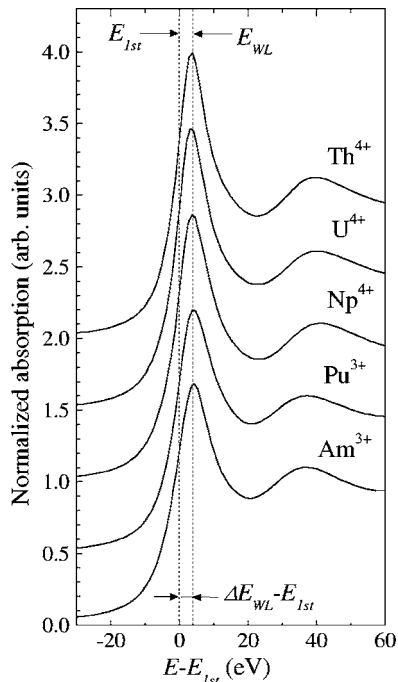


FIG. 3. L_3 near-edge structures of the An^{n+} hydrates, aligned according $E-E_{1st}$, where E is the photon energy and E_{1st} is taken from the first derivative of the spectrum. E_{WL} is the white line maximum.

maximum of the double-electron excitation E_f and E_{1st} . Due to the edgelike structure of the shake-up effect, as discussed later in Sec. III C, E_S needs a correction for the energy difference between the white line maximum E_{WL} and E_{1st} . This energy difference, ΔE_{WL-1st} , is included in the estimation according $E_S = E_f - E_{1st} - \Delta E_{WL-1st}$. ΔE_{WL-1st} of the double-electron excitation is assumed to be similar to the L_3 edge. The values of ΔE_{WL-1st} at the L_3 edges are given in Table III and the resulting E_S is given in Table IV. In order to assign the shake-up process to the experimental value E_S , a comparison with the electron energies in presence of the $2p_{3/2}$ core-hole is required. The relaxation of an atom due to core-hole creation is usually described in the frame of the $Z+1$ approximation. Although SCF models are able to provide reasonable energy corrections, the previously described double excitations are already in good agreement with the $Z+1$ model.^{35,36} Tabulated bonding energies of shells close to the ionization limit are rather scarce for actinides. The energies for this study were taken from Porter and Freedman,³⁷ without a correction for the chemical shift. Evidence was found between E_S and the $Z+1$ $4f_{5/2}$ and $4f_{7/2}$ energy level. The related $Z+1$ energies are listed in Table IV. The comparison allows us to assign the spectral feature to an excitation of a core $2p_{3/2}$ electron accompanied by the auto-ionization of a $4f$ electron. This process creates a $[2p_{3/2}4f_{5/2}/4f_{7/2}]$ double hole configuration, or, in the edge terminology, a $L_3N_{6,7}$ resonance. The shake up of one of the 14 $4f$ electrons to the lowest unoccupied MO results in a feature strong enough to be detectable. Double excitation effects from other energy levels were not observed in the spectra. Equivalent LN transitions were observed for Pb

TABLE IV. Values of the for the double excitation onset energies E_S of Th⁴⁺, U⁴⁺, Np⁴⁺, Pu³⁺, and Am³⁺ hydrate at the L_3 -absorption edge and the related $Z+1$ $4f$ energies taken from Porter and Freedman (Ref. 37). All values are given in eV.

Z	An^{n+}	E_S	$Z+1$	
			$N_6 (4f_{5/2})$	$N_7 (4f_{7/2})$
90	Th ⁴⁺	373.4	366	355
92	U ⁴⁺	419.2	414	403
93	Np ⁴⁺	443.7	436	424
94	Pu ³⁺	456.5	461	446
95	Am ³⁺	478.3	484	470

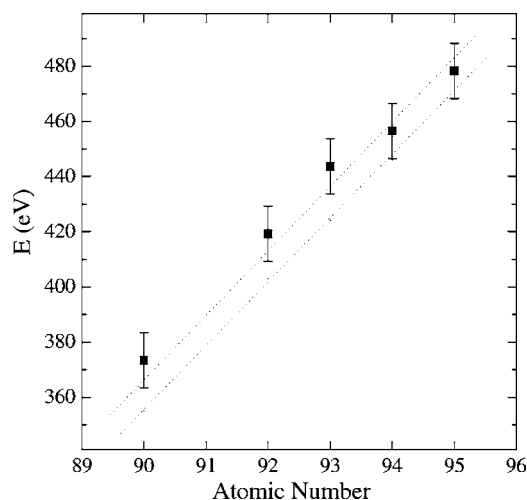


FIG. 4. Experimental energy for the shake-up feature (square dots) in comparison with the $Z+1$ $4f_{5/2}$ and $4f_{7/2}$ energy (dotted line). The error bars represent absolute errors, while the relative errors are in the dimension of the data points.

(Ref. 38) and Hg vapor samples,³⁹ where the $4f$ shell is already completely occupied. There, the double-electron excitations affect only the background slope. In contrast to these spectra, the LN transitions in actinides are sharp.

Figure 4 shows the experimental energy for the shake-up feature in comparison with the $Z+1$ $4f_{5/2}$ and $4f_{7/2}$ energies. For Pa, $Z=91$, no experimental value is available. The only reported spectrum does not reach the energy predicted for the shake-up effect.⁴⁰ The experimental and theoretical values show the same slope except for an energy shift between An^{4+} and An^{3+} . This effect indicates that the shake-up feature may undergo a shift in the range of $\sim 5-8$ eV. This value is higher as the chemical shift observed between An^{4+} and An^{3+} at the x-ray L_3 absorption edge which is in the order of ~ 2 eV. A similar effect was observed between the K and KL edges of the third period atoms⁸ where the chemical shift of the KL edge is significant larger than that at the K edge.

C. Fine structure

The fine structure of the double-electron excitation was investigated using the Th^{4+} hydrate. Th^{4+} has been chosen because it exists exclusively in a single oxidation state. Figure 5 shows the k^3 weighted extended x-ray absorption fine structure at the L_1 , L_2 , and L_3 edges. A dotted line indicates the onsets of the double-electron excitation. The EXAFS oscillations show a π phase shift between the $L_{2,3}$ and L_1 edges. Due to this π shift, the EXAFS signal and the double-electron excitation superimpose in a different manner. At the $L_{2,3}$ edges, the double-electron feature is located at an oscillation maximum and at the L_1 edge at a minimum. The double-electron features were separated from the spectra by subtracting the corresponding EXAFS fit curve (fit parameters are given in Table V). In Fig. 6 the cross sections of the absorption edges and the double-electron features are compared. The $L_{2,3}$ edges comprises an intense well-pronounced resonance, whereas the L_1 edge shows no clear resonance

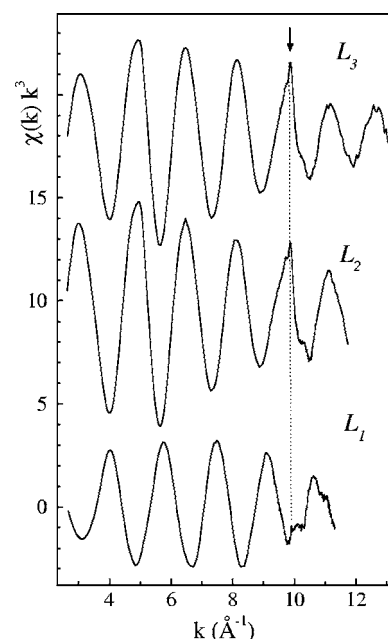


FIG. 5. Experimental k^3 weighted extended x-ray absorption fine structure at the L_1 , L_2 , and L_3 edge of Th^{4+} hydrate. The dotted line indicates the maxima of double-electron excitations. The double-electron features, separated from their corresponding EXAFS signal, are shown in Fig. 6.

structure. The double-electron transition reproduce these spectral features: the $L_2N_{6,7}$ and $L_3N_{6,7}$ show a significant resonance, which is absent in the $L_1N_{6,7}$ transition. It is obvious, that the transition matrix element has the same character for the corresponding L and LN edges. The white line intensity relation of $L:LN$ is $\sim 10^3$ for all three edges. The full width of half maximum of L_2 and L_3 white lines are 10.3 and 8.9 eV, respectively. A fit of the white line at the $L_2N_{6,7}$ and the $L_3N_{6,7}$ double-electron excitation with an Lorentz function reveals line widths of 13.4 and 13.3 eV. It indicates that the double-electron excitation line width is affected from both, the core-hole live time of the L and the N states. The $L_1N_{6,7}$ transition is too noisy for quantitative analysis.

Similar differences in the resonance intensity as at $L_{2,3}$ and the L_1 edges were observed in the XANES spectra of actinides in different oxidation states. Figure 1 has been shown different Np L_3 -edge EXAFS spectra. There, the Np^{4+} spectrum shows a well-pronounced double-electron resonance, whereas the spectra of Np^{5+} , Np^{6+} , and Np^{7+} show less intense features. The intensity relation of these $L_3N_{6,7}$ features corresponds well with the resonance intensity of the L_3 -edge XANES spectra, shown in Fig. 7.

TABLE V. EXAFS structural parameters for Th^{4+} species.

Edge	Shell	R [\AA]	N_{ij}	σ^2 [10^{-2}\AA^2]
L_1	Th-O	2.449 ± 0.007	9.1 ± 0.8	0.65 ± 0.04
L_2	Th-O	2.447 ± 0.004	9.7 ± 0.7	0.64 ± 0.03
L_3	Th-O	2.442 ± 0.004	9.8 ± 0.7	0.68 ± 0.03
$S_0^2 = 0.9$				

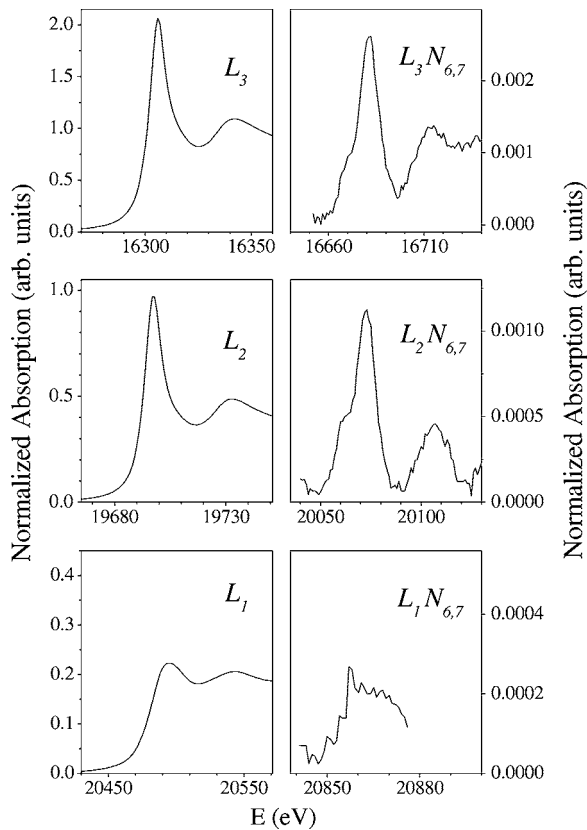


FIG. 6. Comparison of the L_1 , L_2 , and L_3 edge of Th^{4+} hydrate (left side) and the corresponding double-electron features (right side), separated from their EXAFS signals shown in Fig. 5.

D. Consequences for EXAFS data analysis

The double-excitation affects the EXAFS signal and can influence the data analysis. An excitation of a second electron reduces the transition probability in the main scattering path and opens a new one. This may affect especially the integral scattering amplitude for $E \geq E_f$. Therefore, the coordination numbers N_{ij} , extracted from the amplitude function, is expected to be influenced. In contrast, there is no correlation of the double-electron excitation to the origin of the wave vector $E_{k=0}$. Therefore, the influence on R , which is extracted from the phase function, is not expected to be significant. A second effect may occur in the data extraction process. The atomic background signal $\mu_0(E)$ is usually approximated by a spline function that equilibrates the EXAFS oscillations. This estimation might be affected either if the

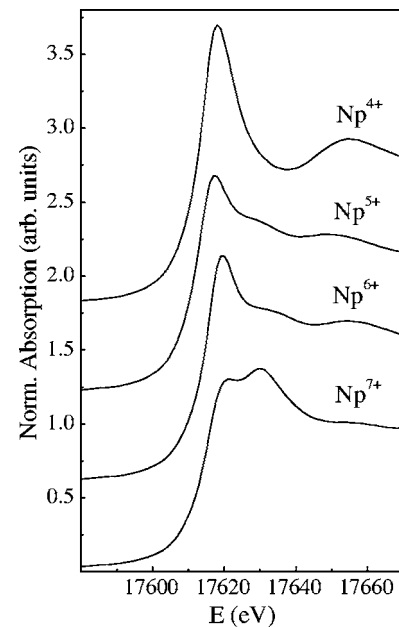


FIG. 7. Np L_3 -edge XANES of Np^{4+} , Np^{5+} , Np^{6+} , and Np^{7+} (same samples as shown in Fig. 1).

EXAFS oscillation is very weak in comparison to the double-electron feature or if the multielectron resonance is in coincidence with a maximum of the EXAFS oscillation. For example, the L_3 edge EXAFS spectrum of Th^{4+} hydrate represents such a superposition of the $L_3N_{6,7}$ double-electron excitation with an EXAFS oscillation maximum. It is well known, that deviations between $\mu_0(E)$ and the spline function lead to artificial peaks at $R \leq 1.2 \text{ \AA}$. There exist at least two concepts to avoid this problem. One possibility is, to subtract the double-electron excitation as a step function. Applications are given for the L_3 spectra of lanthanides.⁴¹ A second solution is to suppress the artificial peak at $R \leq 1.2 \text{ \AA}$ within the spline optimization. Such a procedure is available in most of the recent EXAFS programs, e.g., Ref. 14.

ACKNOWLEDGMENTS

The author thanks M. A. Denecke, K. H. Hallmeier, A. Kodre, and J. Padežnik Gomilšek for hints and fruitful discussions. The measurement of U^{4+} hydrate was performed with an *in situ* spectroelectrochemical cell in the frame of a project supported by the Deutsche Forschungsgemeinschaft under Grant No. HE 2297/2-1.

¹J. M. Esteva, B. Gauthé, P. Dhez, and C. R. Karnatak, J. Phys. B **16**, L263 (1983).

²M. Deutsch and P. Kizler, Phys. Rev. A **45**, 2112 (1992).

³R. D. Deslattes, R. E. LaVilla, P. L. Cowan, and A. Henins, Phys. Rev. A **27**, 923 (1983).

⁴E. Bernieri and E. Burattini, Phys. Rev. A **35**, 3322 (1987).

⁵K. Zhang, E. A. Stern, J. J. Rehr, and F. Ellis, Phys. Rev. B **44**,

2030 (1991).

⁶T. Åberg, Phys. Rev. A **2**, 1726 (1970).

⁷A. Filipponi, E. Bernieri, and S. Mobilio, Phys. Rev. B **38**, 3298 (1988).

⁸A. Filipponi, T. A. Tyson, K. O. Hodgson, and S. Mobilio, Phys. Rev. A **48**, 1328 (1993).

⁹P. D'Angelo, P.-E. Petit, and N. V. Pavel, J. Phys. Chem. B **108**,

- 11857 (2004).
- ¹⁰P. D'Angelo, A. Di Cicco, A. Filipponi, and N. V. Pavel, *Phys. Rev. A* **47**, 2055 (1993).
- ¹¹J. Chaboy, A. Marcelli, and T. A. Tyson, *Phys. Rev. B* **49**, 11652 (1994).
- ¹²J. A. Solera, J. García, and M. G. Proietti, *Phys. Rev. B* **51**, 2678 (1995).
- ¹³W. Matz, N. Schell, G. Bernhard, F. Prokert, T. Reich, J. Claußner, W. Oehme, R. Schlenk, S. Dienel, H. Funke, F. Eichhorn, M. Betzl, D. Pröhl, U. Strauch, G. Hüttig, H. Krug, W. Neumann, V. Brendler, P. Reichel, M. A. Denecke, and H. Nitsche, *Synchrotron Radiat.* **6**, 1076 (1999).
- ¹⁴T. Ressler, *J. Synchrotron Radiat.* **5**, 118 (1998).
- ¹⁵G. N. George and I. J. Pickering, *EXAFSPAK, a suite of computer programs for analysis of x-ray absorption spectra* (Stanford Synchrotron Radiation Laboratory, Stanford (2000)).
- ¹⁶A. L. Ankudinov, B. Ravel, J. J. Rehr, and S. D. Conradson, *Phys. Rev. B* **58**, 7565 (1998).
- ¹⁷T. Reich, G. Bernhard, G. Geipel, H. Funke, C. Hennig, A. Rossberg, W. Matz, N. Schell, and H. Nitsche, *Radiochim. Acta* **88**, 633 (2000).
- ¹⁸H. Bolvin, U. Wahlgren, H. Moll, T. Reich, G. Geipel, T. Fanghänel, and I. Grenthe, *J. Phys. Chem. A* **105**, 11441 (2001).
- ¹⁹C. Hennig, J. Tutschku, A. Rossberg, G. Bernhard, and A. C. Scheinost, *Inorg. Chem.* **44**, 6655 (2005).
- ²⁰J. Padežnik Gomilšek, A. Kodre, I. Arčon, and M. Hribar, *Phys. Rev. A* **68**, 042505 (2003).
- ²¹A. Filipponi, L. Ottaviano, and T. A. Tyson, *Phys. Rev. A* **48**, 2098 (1993).
- ²²J. J. Rehr and R. C. Albers, *Phys. Rev. B* **41**, 8139 (1990).
- ²³C. Den Auwer, D. Guillaumont, P. Guilbaud, S. D. Conradson, J. J. Rehr, A. Ankudinov, and E. Simoni, *New J. Chem.* **28**, 929 (2004).
- ²⁴R. G. Denning, *Structure and Bonding* (Springer-Verlag, Heidelberg, 1992), Vol. 79, Chap. Electronic Structure and Bonding in Actinyl Ions, p. 217.
- ²⁵J. Rothe, M. A. Denecke, V. Neck, R. Müller, and J. I. Kim, *Inorg. Chem.* **41**, 249 (2002).
- ²⁶M. A. Denecke, K. Dardenne, and C. M. Marquardt, *Talanta* **65**, 1008 (2005).
- ²⁷T. Stumpf, C. Hennig, A. Bauer, M. A. Denecke, and T. Fanghänel, *Radiochim. Acta* **92**, 133 (2004).
- ²⁸H. Bolvin, U. Wahlgren, H. Moll, T. Reich, G. Geipel, T. Fanghänel, and I. Grenthe, *J. Phys. Chem. A* **105**, 11441 (2001).
- ²⁹M. R. Antonio, L. Soderholm, C. W. Williams, J.-P. Blaudeau, and B. E. Bursten, *Radiochim. Acta* **89**, 17 (2001).
- ³⁰S. J. Schaphorst, A. F. Kodre, J. Ruschinski, B. Crasemann, T. Åberg, J. Tulkki, M. H. Chen, Y. Azuma, and G. S. Brown, *Phys. Rev. A* **47**, 1953 (1993).
- ³¹J. Petiau, G. Calas, D. Petitmaire, A. Bianconi, M. Benfatto, and A. Marcelli, *Phys. Rev. B* **34**, 7350 (1986).
- ³²P. D'Angelo, N. V. Pavel, D. Roccatano, and H. F. Nolting, *Phys. Rev. B* **54**, 12129 (1996).
- ³³A. L. Ankudinov, S. D. Conradson, J. Mustre de Leon, and J. J. Rehr, *Phys. Rev. B* **57**, 7518 (1998).
- ³⁴A. L. Ankudinov, B. Ravel, J. J. Rehr, and S. D. Conradson, *Phys. Rev. B* **58**, 7565 (1998).
- ³⁵A. Filipponi, *Physica B* **208**, 29 (1995).
- ³⁶J. Chaboy and T. A. Tyson, *Phys. Rev. B* **49**, 5869 (1994).
- ³⁷F. T. Porter and M. S. Freedman, *J. Phys. Chem. Ref. Data* **7**, 1267 (1978).
- ³⁸G. Li, F. Bridges, and G. S. Brown, *Phys. Rev. Lett.* **68**, 1609 (1992).
- ³⁹A. Filipponi, L. Ottaviano, and T. A. Tyson, *Phys. Rev. A* **48**, 2098 (1993).
- ⁴⁰C. Le Naour, D. Trubert, M. V. Di Giandomenico, C. Fillaux, C. Den Auwer, P. Moisy, and C. Hennig, *Inorg. Chem.* **44**, 9542 (2005).
- ⁴¹P. D'Angelo, A. Di Cicco, A. Filipponi, and N. V. Pavel, *Phys. Rev. A* **47**, 2055 (1993).
- ⁴²R. D. Deslattes, E. G. Kessler, Jr., P. Indelicato, L. de Billy, E. Lindroth, and J. Anton, *Rev. Mod. Phys.* **75**, 35 (2003).